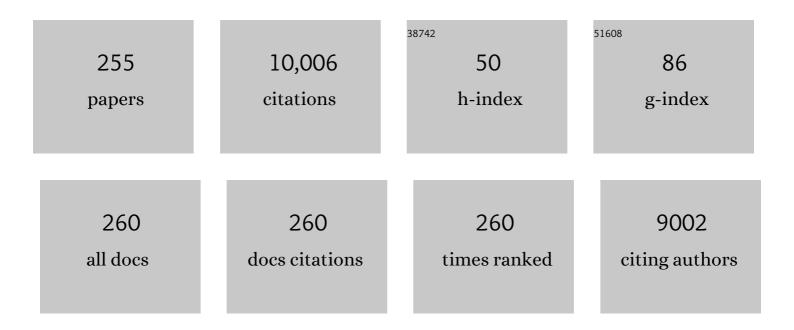
David A Saloner

List of Publications by Year in descending order

Source: https://exaly.com/author-pdf/5740911/publications.pdf Version: 2024-02-01



#	Article	IF	CITATIONS
1	Intracranial Vessel Wall MRI: Principles and Expert Consensus Recommendations of the American Society of Neuroradiology. American Journal of Neuroradiology, 2017, 38, 218-229.	2.4	457
2	Aneurysm Growth Occurs at Region of Low Wall Shear Stress. Stroke, 2008, 39, 2997-3002.	2.0	446
3	High-Resolution CT Imaging of Carotid Artery Atherosclerotic Plaques. American Journal of Neuroradiology, 2008, 29, 875-882.	2.4	319
4	Imaging biomarkers of vulnerable carotid plaques for stroke risk prediction and their potential clinical implications. Lancet Neurology, The, 2019, 18, 559-572.	10.2	279
5	Carotid Artery Wall Imaging: Perspective and Guidelines from the ASNR Vessel Wall Imaging Study Group and Expert Consensus Recommendations of the American Society of Neuroradiology. American Journal of Neuroradiology, 2018, 39, E9-E31.	2.4	213
6	Phaseâ€contrast magnetic resonance imaging measurements in intracranial aneurysms in vivo of flow patterns, velocity fields, and wall shear stress: Comparison with computational fluid dynamics. Magnetic Resonance in Medicine, 2009, 61, 409-417.	3.0	196
7	Giant Intracranial Aneurysms. Neurosurgery, 2011, 69, 1261-1271.	1.1	187
8	Cardiovascular magnetic resonance phase contrast imaging. Journal of Cardiovascular Magnetic Resonance, 2015, 17, 71.	3.3	184
9	MRI-based finite-element analysis of left ventricular aneurysm. American Journal of Physiology - Heart and Circulatory Physiology, 2005, 289, H692-H700.	3.2	179
10	Numerical Analysis of Flow Through a Severely Stenotic Carotid Artery Bifurcation. Journal of Biomechanical Engineering, 2002, 124, 9-20.	1.3	171
11	Flow Residence Time and Regions of Intraluminal Thrombus Deposition in Intracranial Aneurysms. Annals of Biomedical Engineering, 2010, 38, 3058-3069.	2.5	164
12	Assessment of carotid artery stenosis by ultrasonography, conventional angiography, and magnetic resonance angiography: Correlation with ex vivo measurement of plaque stenosis. Journal of Vascular Surgery, 1995, 21, 82-89.	1.1	144
13	Clinical evaluation of aortic coarctation with 4D flow MR imaging. Journal of Magnetic Resonance Imaging, 2010, 31, 711-718.	3.4	137
14	Influence of stenosis morphology on flow through severely stenotic vessels: implications for plaque rupture. Journal of Biomechanics, 2000, 33, 443-455.	2.1	132
15	Numerical Modeling of the Flow in Intracranial Aneurysms: Prediction of Regions Prone to Thrombus Formation. Annals of Biomedical Engineering, 2008, 36, 1793-1804.	2.5	129
16	Magnetic Resonance Measurement of Turbulent Kinetic Energy for the Estimation of Irreversible Pressure Loss in Aortic Stenosis. JACC: Cardiovascular Imaging, 2013, 6, 64-71.	5.3	122
17	Comparison of fourâ€dimensional flow parameters for quantification of flow eccentricity in the ascending aorta. Journal of Magnetic Resonance Imaging, 2011, 34, 1226-1230.	3.4	121
18	Experimental Flow Studies in Exact-Replica Phantoms of Atherosclerotic Carotid Bifurcations Under Steady Input Conditions. Journal of Biomechanical Engineering, 2003, 125, 38-48.	1.3	119

#	Article	IF	CITATIONS
19	Structure of Plaque at Carotid Bifurcation: High-Resolution MRI With Histological Correlation. Stroke, 2001, 32, 2516-2521.	2.0	118
20	Shape Memory Polymer Stent With Expandable Foam: A New Concept for Endovascular Embolization of Fusiform Aneurysms. IEEE Transactions on Biomedical Engineering, 2007, 54, 1157-1160.	4.2	111
21	Atheroemboli to the brain: Size threshold for causing acute neuronal cell death. Journal of Vascular Surgery, 2000, 32, 68-76.	1.1	109
22	First Finite Element Model of the Left Ventricle With Mitral Valve: Insights Into Ischemic Mitral Regurgitation. Annals of Thoracic Surgery, 2010, 89, 1546-1553.	1.3	109
23	Evaluation of myocardial perfusion abnormalities with gadolinium-enhanced snapshot MR imaging in humans. Work in progress Radiology, 1992, 185, 795-801.	7.3	104
24	Intracranial timeâ€ofâ€flight MR angiography at 7T with comparison to 3T. Journal of Magnetic Resonance Imaging, 2007, 26, 900-904.	3.4	104
25	Vascular Imaging With Ferumoxytol as a Contrast Agent. American Journal of Roentgenology, 2015, 205, W366-W373.	2.2	104
26	Cerebral Ischemia and Infarction From Atheroemboli <100 μm in Size. Stroke, 2003, 34, 1976-1980.	2.0	99
27	Multicenter Safety and Practice for Off-Label Diagnostic Use of Ferumoxytol in MRI. Radiology, 2019, 293, 554-564.	7.3	99
28	Macrophage Imaging Within Human Cerebral Aneurysms Wall Using Ferumoxytol-Enhanced MRI: A Pilot Study. Arteriosclerosis, Thrombosis, and Vascular Biology, 2012, 32, 1032-1038.	2.4	98
29	Correlation between lumenal geometry changes and hemodynamics in fusiform intracranial aneurysms. American Journal of Neuroradiology, 2005, 26, 2357-63.	2.4	91
30	Computational approach to quantifying hemodynamic forces in giant cerebral aneurysms. American Journal of Neuroradiology, 2003, 24, 1804-10.	2.4	88
31	Numerical Simulations of Flow in Cerebral Aneurysms: Comparison of CFD Results and In Vivo MRI Measurements. Journal of Biomechanical Engineering, 2008, 130, 051011.	1.3	82
32	Bypass Surgery for the Treatment of Dolichoectatic Basilar Trunk Aneurysms. Neurosurgery, 2016, 79, 83-99.	1.1	82
33	Modern meningioma imaging techniques. Journal of Neuro-Oncology, 2010, 99, 333-340.	2.9	81
34	Silent Intralesional Microhemorrhage as a Risk Factor for Brain Arteriovenous Malformation Rupture. Stroke, 2012, 43, 1240-1246.	2.0	78
35	MRI hemodynamic markers of progressive bicuspid aortic valveâ€related aortic disease. Journal of Magnetic Resonance Imaging, 2014, 40, 140-145.	3.4	78
36	A Computationally Efficient Formal Optimization of Regional Myocardial Contractility in a Sheep With Left Ventricular Aneurysm. Journal of Biomechanical Engineering, 2009, 131, 111001.	1.3	73

#	Article	IF	CITATIONS
37	Major carotid plaque surface irregularities correlate with neurologic symptoms. Journal of Vascular Surgery, 2002, 35, 741-747.	1.1	68
38	Magnetic resonance imaging-based finite element stress analysis after linear repair of left ventricular aneurysm. Journal of Thoracic and Cardiovascular Surgery, 2008, 135, 1094-1102.e2.	0.8	68
39	Measurement of internal carotid artery stenosis from source MR angiograms Radiology, 1994, 193, 219-226.	7.3	66
40	Estimating the Hemodynamic Impact of Interventional Treatments of Aneurysms. Neurosurgery, 2006, 59, E429-E430.	1.1	65
41	Imaging Biomarkers of Aortic Disease. Journal of the American College of Cardiology, 2012, 60, 356-357.	2.8	62
42	Discrimination of Myocardial Acute and Chronic (Scar) Infarctions on Delayed Contrast Enhanced Magnetic Resonance Imaging With Intravascular Magnetic Resonance Contrast Media. Journal of the American College of Cardiology, 2006, 48, 1961-1968.	2.8	60
43	Atherosclerotic Plaque Progression in Carotid Arteries: Monitoring with High-Spatial-Resolution MR Imaging—Multicenter Trial. Radiology, 2009, 252, 789-796.	7.3	59
44	High resolution imaging of the intracranial vessel wall at 3 and 7ÂT using 3D fast spin echo MRI. Magnetic Resonance Materials in Physics, Biology, and Medicine, 2016, 29, 559-570.	2.0	59
45	Carotid plaque computed tomography imaging in stroke and nonstroke patients. Annals of Neurology, 2008, 64, 149-157.	5.3	58
46	Vascular Remodeling in Autogenous Arterio-Venous Fistulas by MRI and CFD. Annals of Biomedical Engineering, 2013, 41, 657-668.	2.5	56
47	Contrast material–enhanced MRA overestimates severity of carotid stenosis, compared with 3D time-of-flight MRA. Journal of Vascular Surgery, 2003, 38, 36-40.	1.1	55
48	Magnetic Resonance Angiography for Free Fibula Flap Transfer. Journal of Reconstructive Microsurgery, 2007, 23, 205-211.	1.8	55
49	Regional Left Ventricular Myocardial Contractility and Stress in a Finite Element Model of Posterobasal Myocardial Infarction. Journal of Biomechanical Engineering, 2011, 133, 044501.	1.3	54
50	Ex-vivo imaging and plaque type classification of intracranial atherosclerotic plaque using high resolution MRI. Atherosclerosis, 2016, 249, 10-16.	0.8	54
51	The AAPM/RSNA physics tutorial for residents. An introduction to MR angiography Radiographics, 1995, 15, 453-465.	3.3	51
52	The Effect of Mitral Annuloplasty Shape in Ischemic Mitral Regurgitation: A Finite Element Simulation. Annals of Thoracic Surgery, 2012, 93, 776-782.	1.3	51
53	USPIO-enhanced MR Angiography of Arteriovenous Fistulas in Patients with Renal Failure. Radiology, 2012, 265, 584-590.	7.3	50
54	Identification of high-risk plaque features in intracranial atherosclerosis: initial experience using a radiomic approach. European Radiology, 2018, 28, 3912-3921.	4.5	50

#	Article	IF	CITATIONS
55	Ferumoxytol-Enhanced MRI to Image Inflammation Within Human Brain Arteriovenous Malformations: a Pilot Investigation. Translational Stroke Research, 2012, 3, 166-173.	4.2	48
56	Diagnosing ulnar neuropathy at the elbow using magnetic resonance neurography. Skeletal Radiology, 2012, 41, 401-407.	2.0	48
57	Vascular Dynamics of a Shape Memory Polymer Foam Aneurysm Treatment Technique. Annals of Biomedical Engineering, 2007, 35, 1870-1884.	2.5	47
58	Clinical Significance of Intraplaque Hemorrhage in Low- and High-Grade Basilar Artery Stenosis on High-Resolution MRI. American Journal of Neuroradiology, 2018, 39, 1286-1292.	2.4	47
59	Intraluminal Thrombus Predicts Rapid Growth of Abdominal Aortic Aneurysms. Radiology, 2020, 294, 707-713.	7.3	47
60	Carotid Atheroma Rupture Observed In Vivo and FSI-Predicted Stress Distribution Based on Pre-rupture Imaging. Annals of Biomedical Engineering, 2010, 38, 2748-2765.	2.5	46
61	Merging computational fluid dynamics and 4D Flow MRI using proper orthogonal decomposition and ridge regression. Journal of Biomechanics, 2017, 58, 162-173.	2.1	46
62	Systolic Flow Displacement Correlates With Future Ascending Aortic Growth in Patients With Bicuspid Aortic Valves Undergoing Magnetic Resonance Surveillance. Investigative Radiology, 2014, 49, 635-639.	6.2	45
63	Ascending thoracic aortic aneurysm wall stress analysis using patient-specific finite element modeling of <i>in vivo</i> magnetic resonance imaging. Interactive Cardiovascular and Thoracic Surgery, 2015, 21, 471-480.	1.1	45
64	MR imaging of flow through tortuous vessels: A numerical simulation. Magnetic Resonance in Medicine, 1994, 31, 184-195.	3.0	43
65	MRI in guiding and assessing intramyocardial therapy. European Radiology, 2005, 15, 851-863.	4.5	43
66	MR Assessment of Myocardial Perfusion, Viability, and Function after Intramyocardial Transfer of VM202, a New Plasmid Human Hepatocyte Growth Factor in Ischemic Swine Myocardium. Radiology, 2008, 249, 107-118.	7.3	43
67	Comparison of the Young-Laplace Law and Finite Element Based Calculation of Ventricular Wall Stress: Implications for Postinfarct and Surgical Ventricular Remodeling. Annals of Thoracic Surgery, 2011, 91, 150-156.	1.3	43
68	Flow patterns in the jugular veins of pulsatile tinnitus patients. Journal of Biomechanics, 2017, 52, 61-67.	2.1	43
69	Transendocardial Delivery of Extracellular Myocardial Markers by Using Combination X-ray/MR Fluoroscopic Guidance: Feasibility Study in Dogs. Radiology, 2004, 231, 689-696.	7.3	42
70	Calculation of the magnetization distribution for fluid flow in curved vessels. Magnetic Resonance in Medicine, 1996, 35, 577-584.	3.0	40
71	Scarred myocardium imposes additional burden on remote viable myocardium despite a reduction in the extent of area with late contrast MR enhancement. European Radiology, 2006, 16, 827-836.	4.5	40
72	Multi-modality cerebral aneurysm haemodynamic analysis: <i>in vivo</i> 4D flow MRI, <i>in vitro</i> volumetric particle velocimetry and <i>in silico</i> computational fluid dynamics. Journal of the Royal Society Interface, 2019, 16, 20190465.	3.4	40

#	Article	IF	CITATIONS
73	Increased Wall Enhancement During Follow-Up as a Predictor of Subsequent Aneurysmal Growth. Stroke, 2020, 51, 1868-1872.	2.0	39
74	Adeno-associated Viral Vector–Encoding Vascular Endothelial Growth Factor Gene: Effect on Cardiovascular MR Perfusion and Infarct Resorption Measurements in Swine. Radiology, 2007, 243, 451-460.	7.3	38
75	Injection of Adeno-associated Viral Vector–Encoding Vascular Endothelial Growth Factor Gene in Infarcted Swine Myocardium: MR Measurements of Left Ventricular Function and Strain. Radiology, 2007, 245, 196-205.	7.3	38
76	Determinants of Image Appearance in Contrast-Enhanced Magnetic Resonance Angiography. Investigative Radiology, 1998, 33, 488-495.	6.2	38
77	Assessment of Vasculature of Meningiomas and the Effects of Embolization with Intra-arterial MR Perfusion Imaging: A Feasibility Study. American Journal of Neuroradiology, 2007, 28, 1771-1777.	2.4	37
78	Asymmetric Mechanical Properties of Porcine Aortic Sinuses. Annals of Thoracic Surgery, 2008, 85, 1631-1638.	1.3	36
79	MR Venous Flow in Sigmoid Sinus Diverticulum. American Journal of Neuroradiology, 2018, 39, 2108-2113.	2.4	36
80	Carotid plaque imaging and the risk of atherosclerotic cardiovascular disease. Cardiovascular Diagnosis and Therapy, 2020, 10, 1048-1067.	1.7	36
81	MR Imaging of Partially Thrombosed Cerebral Aneurysms: Characteristics and Evolution. American Journal of Neuroradiology, 2011, 32, 346-351.	2.4	35
82	Isotropic 3D black blood MRI of abdominal aortic aneurysm wall and intraluminal thrombus. Magnetic Resonance Imaging, 2016, 34, 18-25.	1.8	35
83	Higher Flow Is Present in Unruptured Arteriovenous Malformations With Silent Intralesional Microhemorrhages. Stroke, 2017, 48, 2881-2884.	2.0	35
84	Implantation of 3D-Printed Patient-Specific Aneurysm Models into Cadaveric Specimens: A New Training Paradigm to Allow for Improvements in Cerebrovascular Surgery and Research. BioMed Research International, 2015, 2015, 1-9.	1.9	33
85	Wall stress on ascending thoracic aortic aneurysms with bicuspid compared with tricuspid aortic valve. Journal of Thoracic and Cardiovascular Surgery, 2018, 156, 492-500.	0.8	33
86	Progression of Plaque Burden of Intracranial Atherosclerotic Plaque Predicts Recurrent Stroke/Transient Ischemic Attack: A Pilot Followâ€Up Study Using Higherâ€Resolution <scp>MRI</scp> . Journal of Magnetic Resonance Imaging, 2021, 54, 560-570.	3.4	33
87	Accelerated MRI with CIRcular Cartesian UnderSampling (CIRCUS): a variable density Cartesian sampling strategy for compressed sensing and parallel imaging. Quantitative Imaging in Medicine and Surgery, 2014, 4, 57-67.	2.0	33
88	Magnetic resonance angiography to evaluate septocutaneous perforators in free fibula flap transfer. Journal of Plastic, Reconstructive and Aesthetic Surgery, 2010, 63, 1099-1104.	1.0	32
89	Accelerated whole brain intracranial vessel wall imaging using black blood fast spin echo with compressed sensing (CS-SPACE). Magnetic Resonance Materials in Physics, Biology, and Medicine, 2018, 31, 457-467.	2.0	32
90	MR angiography with a cardiac-phase–specific acquisition window. Journal of Magnetic Resonance Imaging, 1992, 2, 637-643.	3.4	31

#	Article	IF	CITATIONS
91	Magnetic resonance imaging quantification of left ventricular dysfunction following coronary microembolization. Magnetic Resonance in Medicine, 2009, 61, 595-602.	3.0	31
92	Heterogeneous Microinfarcts Caused by Coronary Microemboli: Evaluation with Multidetector CT and MR Imaging in a Swine Model. Radiology, 2010, 254, 718-728.	7.3	31
93	Imaging and modeling of flow in porous media using clinical nuclear emission tomography systems and computational fluid dynamics. Journal of Applied Geophysics, 2012, 76, 74-81.	2.1	31
94	Assessment of turbulent viscous stress using ICOSA 4D Flow MRI for prediction of hemodynamic blood damage. Scientific Reports, 2016, 6, 39773.	3.3	31
95	Vessel Wall–Imaging Biomarkers of Carotid Plaque Vulnerability in StrokeÂPrevention Trials. JACC: Cardiovascular Imaging, 2020, 13, 2445-2456.	5.3	31
96	Comparison of Late Enhancement Cardiovascular Magnetic Resonance and Thallium SPECT in Patients with Coronary Disease and Left Ventricular Dysfunction. Journal of Cardiovascular Magnetic Resonance, 2004, 6, 549-556.	3.3	30
97	MR Guidance of Targeted Injections into Border and Core of Scarred Myocardium in Pigs. Radiology, 2006, 240, 419-426.	7.3	30
98	Segmentation of lumen and outer wall of abdominal aortic aneurysms from 3D black-blood MRI with a registration based geodesic active contour model. Medical Image Analysis, 2017, 40, 1-10.	11.6	30
99	The Reliability of High Resolution MRI in the Measurement of Early Stage Carotid Wall Thickening. Journal of Cardiovascular Magnetic Resonance, 2007, 9, 771-776.	3.3	28
100	Wall enhancement of intracranial saccular and fusiform aneurysms may differ in intensity and extension: a pilot study using 7-T high-resolution black-blood MRI. European Radiology, 2020, 30, 301-307.	4.5	28
101	Dor procedure for dyskinetic anteroapical myocardial infarction fails to improve contractility in the border zone. Journal of Thoracic and Cardiovascular Surgery, 2010, 140, 233-239.e4.	0.8	27
102	Left Ventricular Myocardial Contractility Is Depressed in the Borderzone After Posterolateral Myocardial Infarction. Annals of Thoracic Surgery, 2013, 95, 1619-1625.	1.3	27
103	Large Vessel Arteriopathy After Cranial Radiation Therapy in Pediatric Brain Tumor Survivors. Journal of Child Neurology, 2018, 33, 359-366.	1.4	27
104	Wall stress analyses in patients with ≥5Âcm versus <5Âcm ascending thoracic aortic aneurysm. Journal of Thoracic and Cardiovascular Surgery, 2021, 162, 1452-1459.	0.8	27
105	Left ventricular volume and function after endoventricular patch plasty for dyskinetic anteroapical left ventricular aneurysm in sheep. Journal of Thoracic and Cardiovascular Surgery, 2005, 130, 1032-1038.	0.8	26
106	Computational Fluid Dynamics Within Bifurcated Abdominal Aortic Stent-Grafts. Journal of Endovascular Therapy, 2007, 14, 138-143.	1.5	26
107	Highly accelerated intracranial 4D flow MRI: evaluation of healthy volunteers and patients with intracranial aneurysms. Magnetic Resonance Materials in Physics, Biology, and Medicine, 2018, 31, 295-307.	2.0	26
108	Magnetic resonance angiography of the carotid artery combining two- and three-dimensional acquisitions. Journal of Vascular Surgery, 1992, 16, 609-618.	1.1	25

#	Article	IF	CITATIONS
109	MRA studies of arterial stenosis: Improvements by diastolic acquisition. Magnetic Resonance in Medicine, 1994, 31, 196-203.	3.0	25
110	A numerical study of magnetic resonance images of pulsatile flow in a two dimensional carotid bifurcation. Medical Engineering and Physics, 1998, 20, 643-652.	1.7	25
111	Transitional flows in arterial fluid dynamics. Computer Methods in Applied Mechanics and Engineering, 2007, 196, 3043-3048.	6.6	25
112	Moderate Mitral Regurgitation Accelerates Left Ventricular Remodeling After Posterolateral Myocardial Infarction. Annals of Thoracic Surgery, 2011, 92, 1614-1620.	1.3	25
113	Wall enhancement of intracranial unruptured aneurysm is associated with increased rupture risk and traditional risk factors. European Radiology, 2018, 28, 5019-5026.	4.5	25
114	Roadmap Consensus on Carotid Artery Plaque Imaging and Impact on Therapy Strategies and Guidelines: An International, Multispecialty, Expert Review and Position Statement. American Journal of Neuroradiology, 2021, 42, 1566-1575.	2.4	25
115	Ferumoxytol-Enhanced Magnetic Resonance Angiography is a Feasible Method for the Clinical Evaluation of Lower Extremity Arterial Disease. Annals of Vascular Surgery, 2015, 29, 63-68.	0.9	24
116	Fully automatic segmentation of 4D MRI for cardiac functional measurements. Medical Physics, 2019, 46, 180-189.	3.0	24
117	Significant material property differences between the porcine ascending aorta and aortic sinuses. Journal of Heart Valve Disease, 2008, 17, 606-13.	0.5	24
118	NMR Velocity-Selective Excitation Composites for Flow and Motion Imaging and Suppression of Static Tissue Signal. IEEE Transactions on Medical Imaging, 1987, 6, 141-147.	8.9	23
119	Numerical Simulation of Magnetic Resonance Angiographies of an Anatomically Realistic Stenotic Carotid Bifurcation. Annals of Biomedical Engineering, 2005, 33, 270-283.	2.5	23
120	Endoventricular patch plasty for dyskinetic anteroapical left ventricular aneurysm increases systolic circumferential shortening in sheep. Journal of Thoracic and Cardiovascular Surgery, 2007, 134, 1017-1024.e1.	0.8	23
121	A Novel Method for Quantifying In-Vivo Regional Left Ventricular Myocardial Contractility in the Border Zone of a Myocardial Infarction. Journal of Biomechanical Engineering, 2011, 133, 094506.	1.3	23
122	Scan-Rescan Reproducibility of High Resolution Magnetic Resonance Imaging of Atherosclerotic Plaque in the Middle Cerebral Artery. PLoS ONE, 2015, 10, e0134913.	2.5	23
123	Denoising and spatial resolution enhancement of 4D flow MRI using proper orthogonal decomposition and lasso regularization. Computerized Medical Imaging and Graphics, 2018, 70, 165-172.	5.8	23
124	Semiautomated Characterization of Carotid Artery Plaque Features From Computed Tomography Angiography to Predict Atherosclerotic Cardiovascular Disease Risk Score. Journal of Computer Assisted Tomography, 2019, 43, 452-459.	0.9	23
125	The effect of anteroapical aneurysm plication on end-systolic three-dimensional strain in the sheep: A magnetic resonance imaging tagging study. Journal of Thoracic and Cardiovascular Surgery, 2006, 131, 579-586.e3.	0.8	22
126	Post-stenotic dilation: Evaluation of ascending aortic dilation with 4D flow MR imaging. International Journal of Cardiology, 2012, 156, e40-e42.	1.7	22

#	Article	IF	CITATIONS
127	Assessment of Reynolds stress components and turbulent pressure loss using 4D flow MRI with extended motion encoding. Magnetic Resonance in Medicine, 2018, 79, 1962-1971.	3.0	22
128	Ferumoxytol-enhanced MRI in the peripheral vasculature. Clinical Radiology, 2019, 74, 37-50.	1.1	22
129	4D Flow MRI Pressure Estimation Using Velocity Measurement-Error-Based Weighted Least-Squares. IEEE Transactions on Medical Imaging, 2020, 39, 1668-1680.	8.9	22
130	MR imaging during endovascular procedures: An evaluation of the potential for catheter heating. Magnetic Resonance in Medicine, 2009, 61, 45-53.	3.0	21
131	Central intraluminal saturation stripe on MR angiograms of curved vessels: simulation, phantom, and clinical analysis Radiology, 1996, 198, 733-739.	7.3	20
132	Computational Fluid Dynamics modeling of contrast transport in basilar aneurysms following flow-altering surgeries. Journal of Biomechanics, 2017, 50, 195-201.	2.1	20
133	The manifestation of vortical and secondary flow in the cerebral venous outflow tract: An in vivo MR velocimetry study. Journal of Biomechanics, 2017, 50, 180-187.	2.1	20
134	Non-contrast 3D black blood MRI for abdominal aortic aneurysm surveillance: comparison with CT angiography. European Radiology, 2017, 27, 1787-1794.	4.5	20
135	An efficient two-stage approach for image-based FSI analysis of atherosclerotic arteries. Biomechanics and Modeling in Mechanobiology, 2010, 9, 213-223.	2.8	19
136	Magnetic resonance neurography evaluation of chronic extraspinal sciatica after remote proximal hamstring injury: a preliminary retrospective analysis. Journal of Neurosurgery, 2014, 121, 408-414.	1.6	19
137	Computational Modeling of Flow-Altering Surgeries in Basilar Aneurysms. Annals of Biomedical Engineering, 2015, 43, 1210-1222.	2.5	19
138	Predictive modeling and inÂvivo assessment of cerebral blood flow in the management of complex cerebral aneurysms. Journal of Cerebral Blood Flow and Metabolism, 2016, 36, 998-1003.	4.3	19
139	Highly-accelerated self-gated free-breathing 3D cardiac cine MRI: validation in assessment of left ventricular function. Magnetic Resonance Materials in Physics, Biology, and Medicine, 2017, 30, 337-346.	2.0	19
140	Reduced Jet Velocity in Venous Flow after CSF Drainage: Assessing Hemodynamic Causes of Pulsatile Tinnitus. American Journal of Neuroradiology, 2019, 40, 849-854.	2.4	19
141	Wall enhancement on black-blood MRI is independently associated with symptomatic status of unruptured intracranial saccular aneurysm. European Radiology, 2020, 30, 6413-6420.	4.5	19
142	Wall Stress Distribution in Bicuspid Aortic Valve–Associated Ascending Thoracic Aortic Aneurysms. Annals of Thoracic Surgery, 2020, 110, 807-814.	1.3	19
143	Carotid stent delivery in an XMR suite: immediate assessment of the physiologic impact of extracranial revascularization. American Journal of Neuroradiology, 2005, 26, 531-7.	2.4	19
144	Dedicated coil for carotid MR angiography Radiology, 1990, 176, 868-872.	7.3	18

#	Article	IF	CITATIONS
145	MRI of Geometric and Compositional Features of Vulnerable Carotid Plaque. Stroke, 2007, 38, 637-641.	2.0	18
146	Numerical Simulation of Pre- and Postsurgical Flow in a Giant Basilar Aneurysm. Journal of Biomechanical Engineering, 2008, 130, 021004.	1.3	18
147	Perfusion-CT of developmental venous anomalies: typical and atypical hemodynamic patterns. Journal of Neuroradiology, 2010, 37, 239-242.	1.1	18
148	Feasibility of asymmetric stretch assessment in the ascending aortic wall with DENSE cardiovascular magnetic resonance. Journal of Cardiovascular Magnetic Resonance, 2014, 16, 6.	3.3	18
149	Dilatation of the ascending aorta is associated with presence of aortic regurgitation in patients after repair of tetralogy of Fallot. International Journal of Cardiovascular Imaging, 2016, 32, 1265-1272.	1.5	18
150	Advances in Multimodality Carotid Plaque Imaging: <i>AJR</i> Expert Panel Narrative Review. American Journal of Roentgenology, 2021, 217, 16-26.	2.2	18
151	Application of a connected-voxel algorithm to MR angiographic data. Journal of Magnetic Resonance Imaging, 1991, 1, 423-430.	3.4	17
152	Delivery and assessment of endovascular stents to repair aortic coarctation using MR and X-ray imaging. Journal of Magnetic Resonance Imaging, 2006, 24, 371-378.	3.4	17
153	Highly accelerated aortic 4D flow MR imaging with variable-density random undersampling. Magnetic Resonance Imaging, 2014, 32, 1012-1020.	1.8	17
154	Extended 3D approach for quantification of abnormal ascending aortic flow. Magnetic Resonance Imaging, 2015, 33, 695-700.	1.8	17
155	Cardiac-gated MR angiography of pulsatile flow: K-space strategies. Journal of Magnetic Resonance Imaging, 1995, 5, 297-307.	3.4	16
156	The use of MRI to quantify multi-phase flow patterns and transitions: an application to horizontal slug flow. Nuclear Engineering and Design, 1998, 184, 213-228.	1.7	16
157	Magnetic Resonance Perfusion Tracks 133 Xe Cerebral Blood Flow Changes After Carotid Stenting. Stroke, 2005, 36, 676-678.	2.0	16
158	The distribution and size of ischemic lesions after carotid artery angioplasty and stenting: Evidence for microembolization to terminal arteries. Journal of Vascular Surgery, 2011, 53, 971-976.	1.1	16
159	Surveillance of Unruptured Intracranial Saccular Aneurysms Using Noncontrast 3D-Black-Blood MRI: Comparison of 3D-TOF and Contrast-Enhanced MRA with 3D-DSA. American Journal of Neuroradiology, 2019, 40, 960-966.	2.4	16
160	Estimation of fusiform intracranial aneurysm growth by serial magnetic resonance imaging. Journal of Magnetic Resonance Imaging, 2007, 26, 177-183.	3.4	15
161	MR Physics in Practice. Magnetic Resonance Imaging Clinics of North America, 2015, 23, 1-6.	1.1	15
162	Evaluation of the distribution and progression of intraluminal thrombus in abdominal aortic aneurysms using highâ€resolution MRI. Journal of Magnetic Resonance Imaging, 2019, 50, 994-1001.	3.4	15

#	Article	IF	CITATIONS
163	Self-Gated Free-Breathing 3D Coronary CINE Imaging with Simultaneous Water and Fat Visualization. PLoS ONE, 2014, 9, e89315.	2.5	15
164	Permanent Coronary Artery Occlusion: Cardiovascular MR Imaging Is Platform for Percutaneous Transendocardial Delivery and Assessment of Gene Therapy in Canine Model. Radiology, 2008, 249, 560-571.	7.3	14
165	Left Atrial Transverse Diameter on Computed Tomography Angiography Can Accurately Diagnose Left Atrial Enlargement in Patients With Atrial Fibrillation. Journal of Thoracic Imaging, 2015, 30, 214-217.	1.5	14
166	Deep learning based fully automatic segmentation of the left ventricular endocardium and epicardium from cardiac cine MRI. Quantitative Imaging in Medicine and Surgery, 2021, 11, 1600-1612.	2.0	14
167	Diagnostic Approach to Pulsatile Tinnitus. JAMA Otolaryngology - Head and Neck Surgery, 2022, 148, 476.	2.2	14
168	High Resolution Cine MRI of Vessel Distension. Journal of Computer Assisted Tomography, 1994, 18, 576-580.	0.9	13
169	Reduction of motion artifacts in carotid MRI using freeâ€induction decay navigators. Journal of Magnetic Resonance Imaging, 2014, 40, 214-220.	3.4	13
170	Short term doxycycline treatment induces sustained improvement in myocardial infarction border zone contractility. PLoS ONE, 2018, 13, e0192720.	2.5	13
171	Visualizing wall enhancement over time in unruptured intracranial aneurysms using 3D vessel wall imaging. Journal of Magnetic Resonance Imaging, 2019, 50, 193-200.	3.4	13
172	MR Flow Imaging in Projection Through a Stationary Surround. Journal of Computer Assisted Tomography, 1988, 12, 122-129.	0.9	12
173	Persistent decline in longitudinal and radial strain after coronary microembolization detected on velocity encoded phase contrast magnetic resonance imaging. Journal of Magnetic Resonance Imaging, 2009, 30, 69-76.	3.4	12
174	Extracranial Carotid Artery Stenosis: The Effects on Brain and Cognition with a Focus on Resting‣tate Functional Connectivity. Journal of Neuroimaging, 2020, 30, 736-745.	2.0	12
175	Baseline vessel wall magnetic resonance imaging characteristics associated with in-stent restenosis for intracranial atherosclerotic stenosis. Journal of NeuroInterventional Surgery, 2023, 15, 288-291.	3.3	12
176	Percutaneous transendocardial VEGF gene therapy: MRI guided delivery and characterization of 3D myocardial strain. International Journal of Cardiology, 2010, 143, 255-263.	1.7	11
177	The Benefit of Enhanced Contractility in the Infarct Borderzone: A Virtual Experiment. Frontiers in Physiology, 2012, 3, 86.	2.8	11
178	Gated thoracic magnetic resonance angiography at 3T: noncontrast versus blood pool contrast. International Journal of Cardiovascular Imaging, 2018, 34, 475-483.	1.5	11
179	Assessing the Relationship between Atherosclerotic Cardiovascular Disease Risk Score and Carotid Artery Imaging Findings. Journal of Neuroimaging, 2019, 29, 119-125.	2.0	11
180	Sound Measurement in Patient-Specific 3D Printed Bench Models of Venous Pulsatile Tinnitus. Otology and Neurotology, 2020, 41, e7-e14.	1.3	11

#	Article	IF	CITATIONS
181	A Volumetric Metric for Monitoring Intracranial Aneurysms: Repeatability and Growth Criteria in a Longitudinal MR Imaging Study. American Journal of Neuroradiology, 2021, 42, 1591-1597.	2.4	11
182	Association of diameter and wall stresses of tricuspid aortic valve ascending thoracic aortic antic aneurysms. Journal of Thoracic and Cardiovascular Surgery, 2022, 164, 1365-1375.	0.8	11
183	Quantitative analysis of unruptured intracranial aneurysm wall thickness and enhancement using 7T high resolution, black blood magnetic resonance imaging. Journal of NeuroInterventional Surgery, 2022, 14, 723-728.	3.3	11
184	FLOW AND MOTION. Magnetic Resonance Imaging Clinics of North America, 1999, 7, 699-715.	1.1	11
185	Velocity imaging by rapid cycle tagging. Medical Physics, 1987, 14, 167-171.	3.0	10
186	DETERMINING INTRA-ANEURYSMAL FLOW FOR COILED CEREBRAL ANEURYSMS WITH DIGITAL FLUOROSCOPY. Biomedical Engineering - Applications, Basis and Communications, 2004, 16, 43-48.	0.6	10
187	Semi-automated computer assessment of the degree of carotid artery stenosis compares favorably to visual evaluation. Journal of the Neurological Sciences, 2008, 269, 74-79.	0.6	10
188	Monitoring Serial Change in the Lumen and Outer Wall of Vertebrobasilar Aneurysms. American Journal of Neuroradiology, 2008, 29, 259-264.	2.4	10
189	Moderate Ischemic Mitral Regurgitation After Posterolateral Myocardial Infarction in Sheep Alters Left Ventricular Shear but Not Normal Strain in the Infarct and Infarct Borderzone. Annals of Thoracic Surgery, 2016, 101, 1691-1699.	1.3	10
190	Wall enhancement characteristics of vertebrobasilar nonsaccular aneurysms and their relationship to symptoms. European Journal of Radiology, 2020, 129, 109064.	2.6	10
191	Comparison of 7ÂT and 3ÂT vessel wall MRI for the evaluation of intracranial aneurysm wall. European Radiology, 2022, 32, 2384-2392.	4.5	10
192	Cardiovascular magnetic resonance imaging in delivering and evaluating the efficacy of hepatocyte growth factor gene in chronic infarct scar. Cardiovascular Revascularization Medicine, 2011, 12, 111-122.	0.8	9
193	Proof-of-concept single-arm trial of bevacizumab therapy for brain arteriovenous malformation. BMJ Neurology Open, 2021, 3, e000114.	1.6	9
194	Current status of carotid imaging by MRA. Vascular, 2003, 11, 445-447.	0.5	8
195	Noninvasive MR characterization of structural and functional components of reperfused infarct. Acta Radiologica, 2010, 51, 1093-1102.	1.1	8
196	The regional pattern of abnormal cerebrovascular reactivity in HIV-infected, virally suppressed women. Journal of NeuroVirology, 2020, 26, 734-742.	2.1	8
197	Four dimensional magnetic resonance velocimetry for complex flow in the jugular vein. Quantitative Imaging in Medicine and Surgery, 2015, 5, 635-7.	2.0	8
198	Intensity dependence of flow signal in slice selective velocity measurements. Magnetic Resonance Imaging, 1989, 7, 61-67.	1.8	7

#	Article	IF	CITATIONS
199	Correlating motion of internal organs with the displacements of fiducial markers during respiration. , 2008, , .		7
200	Safety of retained microcatheters: an evaluation of radiofrequency heating in endovascular microcatheters with nitinol, tungsten, and polyetheretherketone braiding at 1.5â€T and 3â€T. Journal of NeuroInterventional Surgery, 2014, 6, 314-319.	3.3	7
201	Surveillance of abdominal aortic aneurysm using accelerated 3D non-contrast black-blood cardiovascular magnetic resonance with compressed sensing (CS-DANTE-SPACE). Journal of Cardiovascular Magnetic Resonance, 2019, 21, 66.	3.3	7
202	On the Relative Impact of Intraluminal Thrombus Heterogeneity on Abdominal Aortic Aneurysm Mechanics. Journal of Biomechanical Engineering, 2019, 141, .	1.3	7
203	Color Doppler artifact from metallic carotid clamp Journal of Ultrasound in Medicine, 1991, 10, 691-694.	1.7	6
204	Assessing the Relationship Between American Heart Association Atherosclerotic Cardiovascular Disease Risk Score and Coronary Artery Imaging Findings. Journal of Computer Assisted Tomography, 2018, 42, 898-905.	0.9	6
205	Extending Cardiac Functional Assessment with Respiratory-Resolved 3D Cine MRI. Scientific Reports, 2019, 9, 11563.	3.3	6
206	Identification and Quantitative Assessment of Different Components of Intracranial Atherosclerotic Plaque by Ex Vivo 3T High-Resolution Multicontrast MRI. American Journal of Neuroradiology, 2017, 38, 1716-1722.	2.4	5
207	Identification of intra-individual variation in intracranial arterial flow by MRI and the effect on computed hemodynamic descriptors. Magnetic Resonance Materials in Physics, Biology, and Medicine, 2021, 34, 659-666.	2.0	5
208	High speed bolus tagging: time resolved velocity quantification of pulsatile flow in a single breath hold. Magnetic Resonance in Medicine, 1994, 32, 661-667.	3.0	4
209	Double-lumen carotid plaque: A morbid configuration. Journal of Vascular Surgery, 2003, 37, 1314-1317.	1.1	4
210	Transport of contrast agents in contrast-enhanced magnetic resonance angiography. Magnetic Resonance Imaging, 2004, 22, 495-504.	1.8	4
211	Reproducibility of quantitative analysis of aortic 4D flow data. Journal of Cardiovascular Magnetic Resonance, 2013, 15, .	3.3	4
212	Ascending thoracic aortic aneurysm growth is minimal at sizes that do not meet criteria for surgical repair. Quantitative Imaging in Medicine and Surgery, 2021, 12, 0-0.	2.0	4
213	Identification of high risk clinical and imaging features for intracranial artery dissection using high-resolution cardiovascular magnetic resonance. Journal of Cardiovascular Magnetic Resonance, 2021, 23, 74.	3.3	4
214	Presence of Vessel Wall Hyperintensity in Unruptured Arteriovenous Malformations on Vessel Wall Magnetic Resonance Imaging: Pilot Study of AVM Vessel Wall "Enhancement― Frontiers in Neuroscience, 2021, 15, 697432.	2.8	4
215	Intra-Arterial MR Perfusion Imaging of Meningiomas: Comparison to Digital Subtraction Angiography and Intravenous MR Perfusion Imaging. PLoS ONE, 2016, 11, e0163554.	2.5	4
216	Current Applications of Magnetic Resonance Vascular Imaging. Cardiology Clinics, 1989, 7, 661-683.	2.2	3

#	Article	IF	CITATIONS
217	Instrumentation for Magnetic Resonance Angiography. CardioVascular and Interventional Radiology, 1992, 15, 14-22.	2.0	3
218	Four dimensional bolus tagging imaging of pulsatile flowâ~†. Magnetic Resonance Imaging, 2000, 18, 1097-1107.	1.8	3
219	Unmasking complicated atherosclerotic plaques on carotid magnetic resonance angiography: A report of three cases. Journal of Vascular Surgery, 2006, 44, 884-887.	1.1	3
220	Imaging and CFD in the analysis of vascular disease progression. , 2006, , .		3
221	Temporal Stability of Dysmorphic Fusiform Aneurysms of the Intracranial Internal Carotid Artery. Journal of Vascular and Interventional Radiology, 2011, 22, 1007-1011.	0.5	3
222	Shape-appearance constrained segmentation and separation of vein and artery in pulsatile tinnitus patients based on MR angiography and flow MRI. Magnetic Resonance Imaging, 2019, 61, 187-195.	1.8	3
223	Carotid Artery Imaging Is More Strongly Associated With the 10-Year Atherosclerotic Cardiovascular Disease Score Than Coronary Artery Imaging. Journal of Computer Assisted Tomography, 2019, 43, 679-685.	0.9	3
224	Left ventricular geometry during unloading and the end-systolic pressure volume relationship: Measurement with a modified real-time MRI-based method in normal sheep. PLoS ONE, 2020, 15, e0234896.	2.5	3
225	Computer-aided quantification of non-contrast 3D black blood MRI as an efficient alternative to reference standard manual CT angiography measurements of abdominal aortic aneurysms. European Journal of Radiology, 2021, 134, 109396.	2.6	3
226	Computational Models of Vascular Mechanics. , 2010, , 99-170.		3
227	Abdominal aortic aneurysm measurement at CT/MRI: potential clinical ramifications of non-standardized measurement technique and importance of multiplanar reformation. Quantitative Imaging in Medicine and Surgery, 2021, 11, 823-830.	2.0	2
228	Association of 3-Year All-Cause Mortality and Peak Wall Stresses of Ascending Thoracic Aortic Antic Aneurysms in Veterans. Seminars in Thoracic and Cardiovascular Surgery, 2023, 35, 447-456.	0.6	2
229	Characterization of surface defects and determination of overlayer nucleation and growth by surface-sensitive diffraction. Applied Surface Science, 1986, 26, 418-430.	6.1	1
230	Techniques for Vascular Depiction Using Magnetic Resonance Angiography. Seminars in Interventional Radiology, 1998, 15, 189-204.	0.8	1
231	Cardiovascular flow patterns: what should we make of them?. , 1999, 15, 97-98.		1
232	Left Ventricular Pressure Gating in Ovine Cardiac Studies: A Software-Based Method. Journal of Biomechanical Engineering, 2013, 135, 34502.	1.3	1
233	Cognitive Imaging. International Journal of Cognitive Informatics and Natural Intelligence, 2018, 12, 1-16.	0.4	1
234	COMPARISON OF TWO METHODS FOR ESTIMATING THE UNLOADED STATE FOR ABDOMINAL AORTIC ANEURYSM STRESS CALCULATIONS. Journal of Mechanics in Medicine and Biology, 2019, 19, 1950015.	0.7	1

#	Article	IF	CITATIONS
235	Intracranial vascular imaging detects arterial wall abnormalities in persons with treated HIV infection. Aids, 2021, Publish Ahead of Print, 69-73.	2.2	1
236	An Experimental Study of Transitional Behavior in Physiological Flow Regimes. , 2006, , .		1
237	Experimental Study of the Vascular Dynamics of a Saccular Basilar Aneurysm. , 2006, , .		1
238	Regional wall stress differences on tricuspid aortic valve-associated ascending aortic aneurysms. Interactive Cardiovascular and Thoracic Surgery, 2022, 34, 1115-1123.	1.1	1
239	Characteristics of Carotid Plaque as Risk Factors for Stroke. Perspectives in Vascular Surgery and Endovascular Therapy, 2004, 16, 193-199.	0.6	Ο
240	Assessment of the potential for catheter heating during MR imaging. , 2008, , .		0
241	Patient Specific FEM Analysis of the Atherosclerotic Carotid Bifurcation. , 2009, , .		Ο
242	Studying contaminant transport and chem ical reduction in subsurface sediment by modeling flow in porous media. , 2010, , .		0
243	Development of a Rapid, High Resolution Magnetic Resonance Imaging Protocol for the Assessment of Arteriovenous Fistula Remodeling. Journal of Vascular Surgery, 2011, 54, 592-593.	1.1	Ο
244	Improved quantification of abnormal aortic flow in 3D compared to standard 2D approach. Journal of Cardiovascular Magnetic Resonance, 2013, 15, P232.	3.3	0
245	Vascular Inflammation in a Growing Iliac Artery Aneurysm. Clinical Nuclear Medicine, 2015, 40, e323-e324.	1.3	Ο
246	Letter by Zhu et al Regarding Article, "Aortic Wall Inflammation Predicts Abdominal Aortic Aneurysm Expansion, Rupture, and Need for Surgical Repair― Circulation, 2018, 137, 1293-1294.	1.6	0
247	Wall Stress Changes in Ascending Thoracic Aortic Aneurysms Do Not Correlate with Changes in Diameter over Time. Journal of the American College of Surgeons, 2020, 231, S49.	0.5	0
248	Growth of common iliac artery aneurysms coexisting with abdominal aortic aneurysms: associated factors and potential role of intraluminal thrombus. Quantitative Imaging in Medicine and Surgery, 2020, 10, 703-712.	2.0	0
249	Quantitative measurement of atheroma burden: reproducibility in serial studies of atherosclerotic femoral arteries. Magnetic Resonance Materials in Physics, Biology, and Medicine, 2020, 33, 855-863.	2.0	Ο
250	A kinematic modelâ€based analysis framework for 3D Cineâ€DENSE—validation with an axially compressed gel phantom and application in sheep before and after anteroâ€apical myocardial infarction. Magnetic Resonance in Medicine, 2021, 86, 2105-2121.	3.0	0
251	Aneurysm Growth and Thrombus Formation in the Basilar Artery. , 2004, , .		0
252	A Method for Developing MRI-Based Finite Element Models of the Left Ventricle With Mitral Valve and Chordae Tendineae. , 2010, , .		0

#	Article	IF	CITATIONS
253	Intracranial Aneurysms: Imaging, Hemodynamics, and Remodeling. , 2018, , 137-167.		Ο
254	Computational Fluid Dynamics for Evaluating Hemodynamics. , 2020, , 331-347.		0
255	Suture Forces for Closure of Transapical Transcatheter Aortic Valve Replacement: A Mathematical Model. Journal of Heart Valve Disease, 2016, 25, 424-429.	0.5	Ο